

Weyl Exceptional Rings in a Three-Dimensional Dissipative Cold Atomic Gas

Yong Xu,^{*} Sheng-Tao Wang, and L.-M. Duan

Department of Physics, University of Michigan, Ann Arbor, Michigan 48109, USA

Three-dimensional topological Weyl semimetals can generally support a zero-dimensional Weyl point characterized by a quantized Chern number or a one-dimensional Weyl nodal ring (or line) characterized by a quantized Berry phase in the momentum space. Here, in a dissipative system with particle gain and loss, we discover a new type of topological ring, dubbed Weyl exceptional ring consisting of exceptional points at which two eigenstates coalesce. Such a Weyl exceptional ring is characterized by both a quantized Chern number and a quantized Berry phase, which are defined via the Riemann surface. We propose an experimental scheme to realize and measure the Weyl exceptional ring in a dissipative cold atomic gas trapped in an optical lattice.

Recently, condensed matter systems have proven to be a powerful platform to study low energy gapless particles by using momentum space band structures to mimic the energy-momentum relation of relativistic particles [1, 2] and beyond [3–6]. One celebrated example in three dimensions is the zero-dimensional Weyl point [7–18] described by the Weyl Hamiltonian, which has been long sought-after in particle physics but only experimentally observed in condensed matter materials [19–21]. Such a Weyl point can be viewed as a magnetic monopole [22] in the momentum space and possesses a quantized Chern number on a surface enclosing the point. Another example is the one-dimensional Weyl nodal ring [3, 23–25], which has no counterpart in particle physics. It can be regarded as the generalization of zero-dimensional Dirac cones in two-dimensional systems, such as in graphene, to three-dimensional systems. Such a nodal ring has a quantized Berry phase over a closed path encircling it but does not possess a nonzero quantized Chern number. This leads to a natural question of whether there exists a topological ring exhibiting both a quantized Chern number and a quantized Berry phase in the momentum space.

So far, studies on those gapless states focus on closed and lossless systems. However, particle gain and loss are generally present in natural systems. Such systems can often be described by non-Hermitian Hamiltonians [26–29], which are widely applied to many different systems [30–40]. Due to the non-Hermiticity, eigenvalues of the Hamiltonian are generically complex unless the \mathcal{PT} symmetry [41] is conserved and the imaginary part of energy is associated with either decay or growth. Another intriguing feature of a non-Hermitian system is the existence of exceptional points (EPs) [26–29] at which two eigenstates coalesce and the Hamiltonian becomes defective, leading to many novel phenomena, such as loss-induced transparency [30], single-mode lasers [36, 37], and reversed pump dependence of lasers [33].

In this paper, we investigate a system of Weyl points in the presence of a spin-dependent non-Hermitian term and find a Weyl exceptional ring composed of EPs. In stark contrast to a Weyl nodal ring [3, 24, 25], which does not have a nonzero Chern number, remarkably, this

ring exhibits a nonzero quantized Chern number as long as the integral of the Berry curvature is evaluated over a surface (labeled by \mathcal{S}) that encloses the whole ring. Since energy is multi-valued in the complex parameter space due to its square root form, a state on the surface \mathcal{S} may be defined over the Riemann surface, on which a function is single valued. On the other hand, the Chern number is zero when the surface \mathcal{S} does not enclose any part of the ring even when it is located inside it. Besides the Chern number, such a Weyl exceptional ring has a quantized Berry phase over a trajectory encircling the ring twice, instead of once in the case of the Weyl nodal ring. Furthermore, we propose a feasible scheme to engineer and probe the Weyl exceptional ring in a dissipative ultracold atomic gas. In such a system, we find that the Fermi arc can still exist but is suppressed, even though the Weyl point transforms into a ring.

Toy model of Weyl exceptional ring—Near a Weyl point in the momentum space, a system can be described by the Weyl Hamiltonian $H_W = \pm \sum_{\nu} v_{\nu} k_{\nu} \sigma_{\nu}$, where σ_{ν} represent Pauli matrices and \pm the chirality. For clarity, we consider the positive chirality and choose $v_{\nu} = 1$ hereafter. In the presence of a non-Hermitian term $i\gamma\sigma_z$ ($\gamma > 0$) associated with particle gain for spin up atoms and loss for spin down ones, the Hamiltonian becomes

$$H(\mathbf{k}) = \sum_{\nu=x,y,z} k_{\nu} \sigma_{\nu} + i\gamma\sigma_z, \quad (1)$$

taking the energy unit to be 1. The eigenvalues are $E_{\theta}(\mathbf{k}) = \sqrt{k^2 - \gamma^2 + 2ik_z\gamma} = \sqrt{A(\mathbf{k})}e^{i\theta/2}$, where $A(\mathbf{k}) = \sqrt{(k^2 - \gamma^2)^2 + 4k_z^2\gamma^2}$ with $k^2 = k_x^2 + k_y^2 + k_z^2$, and θ is defined via $\cos\theta = (k^2 - \gamma^2)/A(\mathbf{k})$ and $\sin\theta = 2k_z\gamma/A(\mathbf{k})$. Here, θ is used to label two branches, given that $e^{i\theta/2}$ gains a minus sign upon $\theta \rightarrow \theta + 2\pi$, corresponding to the other band. In the absence of γ , energy of both bands is real and two bands touch at $\mathbf{k} = 0$ with linear dispersion along all three momentum directions. In this case, θ takes only two nonequivalent discrete values: 0 and 2π (corresponding to two distinct and separate bands). When $\gamma > 0$, the eigenvalues become complex, and the single touching point morphs into a Weyl exceptional ring in the $k_z = 0$ plane characterized

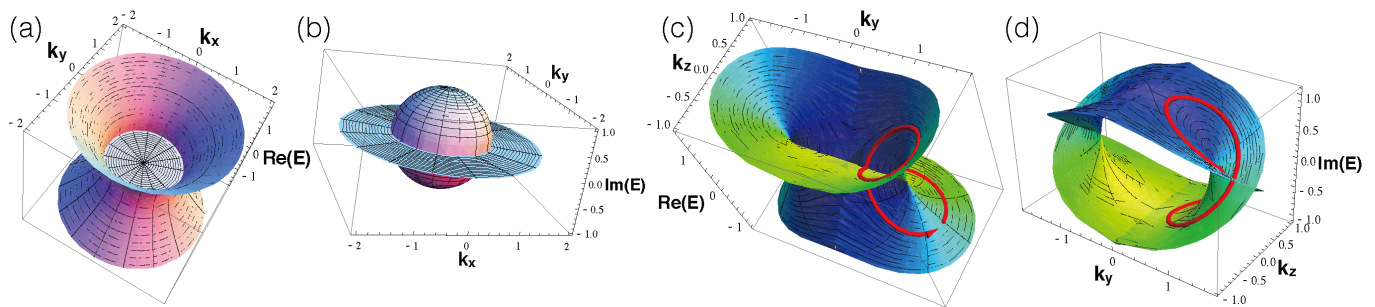


FIG. 1. (Color online) Energy spectra and the Riemann surface of the toy model in Eq. (1). Spectra with respect to k_x and k_y for $k_z = 0$ in (a) (real parts) and (b) (imaginary parts). Real (c) and imaginary parts (d) of the Riemann surface as a function of k_y and k_z for $k_x = 0$. In (c) and (d), the color represents the strength of $\theta \bmod 4\pi$, and the red tube arrow shows a path from $\theta = 0$ to $\theta = 4\pi$.

by $k_x^2 + k_y^2 = \gamma^2$. On this ring, both the real and imaginary parts of the eigenvalues vanish [shown in Fig. 1(a) and (b)] and two eigenstates coalesce into a single one (different from the case of degeneracy). Fig. 1(a) and (b) also illustrate that in the $k_z = 0$ plane energy is purely real outside the ring (with conserved \mathcal{PT} symmetry) and purely imaginary inside it for this simple model. Interestingly, θ takes continuous values from 0 to 4π (θ and $\theta + 4\pi$ are equivalent) and gains 2π when a state travels through the ring and returns, ending up at another state with opposite energy, arising from the role of branch points that the Weyl exceptional ring plays.

In complex analysis, besides using branch cuts, an alternative visual representation to depict a multi-valued function is the Riemann surface, a two-dimensional (2D) manifold that wraps around the complex plane infinite (noncompact) or finite (compact) number of times. Before we discuss the topology of the Weyl exceptional ring, let us first focus on the definition of a closed 2D surface \mathcal{S} via the Riemann surface. In Fig. 1(c) and (d), we plot the Riemann surface of E_θ for $k_x = 0$ (the color represents the strength of $\theta \bmod 4\pi$), showing that energy is single-valued on the surface, which connects the different bands. Given the single value property, we define each state on \mathcal{S} to be living on the Riemann surface. For example, if we consider a state at \mathbf{k}_0 with θ_0 , any other states on the surface \mathcal{S} can be obtained by starting from this state and travelling on the momentum space surface \mathcal{S} while keeping $E_\theta(\mathbf{k})$ on the Riemann surface.

With the proper definition of a closed 2D surface, we can characterize the topology of a Weyl exceptional ring by the Chern number on the surface based on two approaches: the integral of spin vector fields and the Berry curvature. For the former, the Chern number is given by [42]

$$N_3 = \frac{1}{4\pi} \oint_{\mathcal{S}} \mathbf{d}\theta \cdot \left(\frac{\partial \mathbf{d}\theta}{\partial u_1} \times \frac{\partial \mathbf{d}\theta}{\partial u_2} \right) du_1 du_2, \quad (2)$$

which characterizes the number of times that the spin field $\mathbf{d}_\theta = \sum_{\nu=x,y,z} \langle \sigma_\nu \rangle \mathbf{e}_\nu$ wraps around a closed sur-

face \mathcal{S} parametrized by (u_1, u_2) . Here, \mathbf{e}_ν denotes the unit vector along the ν direction and $\langle \sigma_\nu \rangle \equiv \langle u_\theta(\mathbf{k}) | \sigma_\nu | u_\theta(\mathbf{k}) \rangle$ with $|u_\theta(\mathbf{k})\rangle$ being the normalized right eigenstate of $H(\mathbf{k})$ [i.e., $H(\mathbf{k})|u_\theta(\mathbf{k})\rangle = E_\theta(\mathbf{k})|u_\theta(\mathbf{k})\rangle$ and $\langle u_\theta(\mathbf{k}) | u_\theta(\mathbf{k}) \rangle = 1$]. Direct calculations show that $N_3 = \pm 1$ when the surface \mathcal{S} encloses the whole ring as shown in Fig. 2(a), while $N_3 = 0$ when it does not enclose any part of the ring [shown in Fig. 2(b)].

Analogous to the scenario without decay [43], we may also define the first Chern number via the Berry curvature

$$C_2 = \frac{1}{2\pi} \oint_{\mathcal{S}} \boldsymbol{\Omega}_\theta(\mathbf{k}) \cdot d\mathcal{S}, \quad (3)$$

where $\boldsymbol{\Omega}_\theta(\mathbf{k}) = i \langle \nabla_{\mathbf{k}} u_\theta(\mathbf{k}) | \times | \nabla_{\mathbf{k}} u_\theta(\mathbf{k}) \rangle$ is the Berry curvature. Our calculations show that $C_2 = \pm 1$ when the surface \mathcal{S} encloses the Weyl exceptional ring and $C_2 = 0$ otherwise, suggesting that the topological charge is entirely carried by the ring.

The physical meaning of the Berry curvature in this system can be understood from the following semiclassical equation under an external gradient force \mathbf{F} (see the supplemental material for derivation)

$$\begin{aligned} \dot{\mathbf{r}}_c &= \partial_{\mathbf{k}_c} \bar{E}(\mathbf{k}_c) - \dot{\mathbf{k}}_c \times \boldsymbol{\Omega}_\theta(\mathbf{k}_c), \\ \hbar \dot{\mathbf{k}}_c &= \mathbf{F}, \end{aligned} \quad (4)$$

where $\bar{E}(\mathbf{k}_c) = \text{Re}[E_\theta(\mathbf{k}_c)] + \bar{\mathbf{A}}_\theta(\mathbf{k}_c) \cdot \dot{\mathbf{k}}_c$, $\bar{\mathbf{A}}_\theta(\mathbf{k}_c) \equiv \text{Re}[\mathbf{A}_\theta(\mathbf{k}_c) - \dot{\mathbf{A}}_\theta(\mathbf{k}_c)]$ with the Berry connection being $\mathbf{A}_\theta(\mathbf{k}) = i \langle u_\theta(\mathbf{k}) | \partial_{\mathbf{k}} u_\theta(\mathbf{k}) \rangle$ and $\dot{\mathbf{A}}_\theta(\mathbf{k}) = i \langle \tilde{u}_\theta(\mathbf{k}) | \partial_{\mathbf{k}} u_\theta(\mathbf{k}) \rangle$, where $\langle \tilde{u}_\theta(\mathbf{k}) |$ is the normalized left eigenstate of H [i.e., $\langle \tilde{u}_\theta(\mathbf{k}) | H(\mathbf{k}) = \langle \tilde{u}_\theta(\mathbf{k}) | E_\theta(\mathbf{k})$ and $\langle \tilde{u}_\theta(\mathbf{k}) | u_\theta(\mathbf{k}) \rangle = 1$]; \mathbf{r}_c and \mathbf{k}_c are the center coordinate of a wave packet in the real space and momentum space, respectively. Clearly, the Berry curvature plays the same role as in the traditional semiclassical equation in a closed system [44]. However, in this open system, the equation includes a term that effectively modifies the energy spectra, resulting from the difference between left and right eigenstates, a feature in a non-Hermitian Hamiltonian. Without \mathbf{F} , the group velocity is dictated by the real

part of the spectra, which implies that inside the Weyl exceptional ring in the $k_z = 0$ plane, the group velocity vanishes.

Other than the Chern number on the surface, there also exists a quantized Berry phase characterizing the Weyl exceptional ring, defined as

$$C_1 = \oint_{2\mathcal{L}} i \langle \tilde{u}_\theta(\mathbf{k}) | \partial_{\mathbf{k}} u_\theta(\mathbf{k}) \rangle \cdot d\mathbf{k}, \quad (6)$$

where the path $2\mathcal{L}$ travels across the ring twice along the Riemann surface so that the state returns to the original one after the entire trajectory as shown in Fig. 1(c) and (d). Direct calculations yield $C_1 = \pm\pi$, consistent with the result for a single EP [26]. This Berry phase is different from that of a Weyl nodal ring in which the quantized Berry phase is obtained when the trajectory encircles the ring once [3, 24, 25].

Realization in dissipative cold atomic gases—To realize the Weyl exceptional ring in cold atoms, we consider the following model

$$H = \sum_{k_z, \mathbf{x}} \left[(\bar{h}_z + i\gamma) \hat{c}_{k_z, \mathbf{x}}^\dagger \sigma_z \hat{c}_{k_z, \mathbf{x}} + \sum_{\nu=x,y} (-J \hat{c}_{k_z, \mathbf{x}}^\dagger \hat{c}_{k_z, \mathbf{x}+a\mathbf{e}_\nu} + (-1)^{j_x+j_y} J_{SO\nu} \hat{c}_{k_z, \mathbf{x}}^\dagger \sigma_\nu \hat{c}_{k_z, \mathbf{x}+a\mathbf{e}_\nu} + H.c.) + h_0 \right], \quad (7)$$

where $\mathbf{x} = j_x a \mathbf{e}_x + j_y a \mathbf{e}_y$ (with a being the lattice constant) labels the location of sites, $\hat{c}_{k_z, \mathbf{x}}^\dagger = (\hat{c}_{k_z, \mathbf{x}, \uparrow}^\dagger, \hat{c}_{k_z, \mathbf{x}, \downarrow}^\dagger)$ with $\hat{c}_{k_z, \mathbf{x}, \sigma}^\dagger$ ($\hat{c}_{k_z, \mathbf{x}, \sigma}$) being the creation (annihilation) operator, J and $J_{SO\nu}$ ($J_{SOx} = -J_{SOy} = J_{SO}$) stand for the tunneling and spin-orbit coupling strength, $h_0 = [-i\gamma + \hbar^2 k_z^2 / (2m)] \hat{c}_{k_z, \mathbf{x}}^\dagger \hat{c}_{k_z, \mathbf{x}}$, with γ denoting the decay strength, and $\bar{h}_z = \alpha k_z + h_z$ is the effective Zeeman field with $\alpha = \hbar^2 k_{Lz} / (2m)$ where k_{Lz} depends on the wave vector of Raman laser beams along the z direction, m is the mass of atoms, and h_z the Zeeman field proportional to the two-photon detuning. Here, we consider the atoms to be trapped in an optical lattice in the x and y directions while there is no lattice along the z direction.

Without γ , this Hamiltonian, which has two Weyl points and a fourfold degenerate point, can be experimentally engineered by coupling two hyperfine states with two pairs of Raman laser beams in cold atom optical lattices [45]. To generate the decay term representing an atom loss $-2i\gamma$ for spin down atoms, one may consider using a resonant optical beam to kick the atoms in the $|\downarrow\rangle$ state out of a weak trap as shown in Fig. 2(d), which has been experimentally realized in ^6Li [40]. Alternatively, one may consider applying a radio frequency pulse to excite atoms in the $|\downarrow\rangle$ state to another irrelevant state $|3\rangle$, leading to an effective decay for spin down atoms when atoms in $|3\rangle$ experience a loss by applying an anti-trap.

To see the energy spectra, we write down the Hamiltonian in the momentum space,

$$H(\mathbf{k}) = (\bar{h}_z + i\gamma) \sigma_z - h_t \tau_x + \tau_y (-b_x \sigma_x + b_y \sigma_y), \quad (8)$$

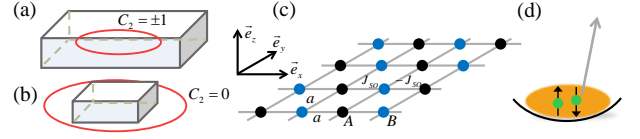


FIG. 2. (Color online) (a) A surface enclosing a Weyl exceptional ring and (b) a surface located inside the ring. (c) Lattice structure in the (x, y) plane. (d) Schematic of trapped atoms being kicked out by a resonant optical beam (denoted by the grey arrow).

in the basis $\Psi(\mathbf{k})^T$ with $\Psi(\mathbf{k}) = (e^{ik_x a} \hat{A}_{\mathbf{k}\uparrow}, e^{ik_x a} \hat{A}_{\mathbf{k}\downarrow}, \hat{B}_{\mathbf{k}\uparrow}, \hat{B}_{\mathbf{k}\downarrow})$, where $\hat{A}_{\mathbf{k}\sigma}$ ($\hat{B}_{\mathbf{k}\sigma}$) annihilates a state with spin σ and momentum \mathbf{k} located at A (B) site [A and B constitute a unit cell as shown in Fig. 2(c)]. Here, $h_t = 2J[\cos(k_x a) + \cos(k_y a)]$, $b_x = 2J_{SO} \sin(k_x a)$ and $b_y = -2J_{SO} \sin(k_y a)$; $\tau_{x,y}$ are Pauli matrices acting on A, B sublattices. This Hamiltonian can be transformed into a block diagonal matrix, i.e., $H \rightarrow H' = (\bar{h}_z + i\gamma) \sigma_z - h_t \sigma_z \tau_z + \tau_z (b_x \sigma_y + b_y \sigma_x)$, which commutes with τ_z . Note that we have neglected the spin-independent term h_0 , which has no essential effects on the physics.

Similar to the toy model in Eq. (1), eigenvalues of this Hamiltonian are $E_{\theta_{\pm}}(\mathbf{k}) = \sqrt{b_{\pm}^2 - \gamma^2 + 2ib_{z\pm}\gamma} = \sqrt{A_{\pm}(\mathbf{k})} e^{i\theta_{\pm}/2}$, where $A_{\pm}(\mathbf{k}) = \sqrt{(b_{\pm}^2 - \gamma^2)^2 + 4b_{z\pm}^2 \gamma^2}$ with $b_{\pm}^2 = b_x^2 + b_y^2 + b_{z\pm}^2$ and $b_{z\pm} = \pm h_t + \bar{h}_z$ (\pm label two particle or hole bands associated with the subspace $\tau_z = \mp$ for H'), and θ_{\pm} are defined by $\cos \theta_{\pm} = (b_{\pm}^2 - \gamma^2) / A_{\pm}(\mathbf{k})$ and $\sin \theta_{\pm} = 2b_{z\pm} \gamma / A_{\pm}(\mathbf{k})$. Without γ , energy is purely real, and Weyl points emerge at $\mathbf{k}_{W0} = (k_x a, k_y a, k_z a_z) = [\pi, 0, -2m\pi h_z / (\hbar^2 k_{Lz}^2)]$ or $\mathbf{k}_{W\pm} = [0, 0, -2m\pi(\pm 4J + h_z) / (\hbar^2 k_{Lz}^2)]$, where $a_z = \pi / k_{Lz}$. The touching point is fourfold (doubly) degenerate at \mathbf{k}_{W0} ($\mathbf{k}_{W\pm}$). When $\gamma > 0$, the spectrum becomes complex and it is purely real only in the plane $b_{z\pm} = 0$. A touching point transforms into a closed line (i.e., Weyl exceptional ring) at which particle and hole bands coalesce when $b_{z\pm} = 0$ and $b_x^2 + b_y^2 = \gamma^2$, as shown in Fig. 3(a). Around \mathbf{k}_{W0} , the fourfold degeneracy of the touching point is broken, and there emerge two Weyl exceptional rings that are not degenerate except at four points with $|\sin k_x a_x| = \gamma / (2\sqrt{2} J_{SO})$, $k_x = \pm k_y - \pi$, and $k_z = -h_z / \alpha$ [as shown in Fig. 3(a)]. Around $\mathbf{k}_{W\pm}$, each Weyl point morphs into a single Weyl exceptional ring, which can be approximated by $k_x^2 + k_y^2 = \gamma^2 / (4J_{SO}^2)$ and $k_z = [-h_z \pm J(4 - \gamma^2 / (4J_{SO}^2))] / \alpha$ when $\gamma \ll 2J_{SO}$.

Analogous to the toy model, a Weyl exceptional ring in this realistic model can be characterized by the Chern number defined in Eq. (3), i.e., evaluated by an integral of the Berry curvature over a closed surface \mathcal{S} via the Riemann surface. Around k_{W0} , there are two Weyl exceptional rings associated with two branches θ_{\pm} , and the Chern number is defined for each band with $C_{\theta_{\pm}} = 1$

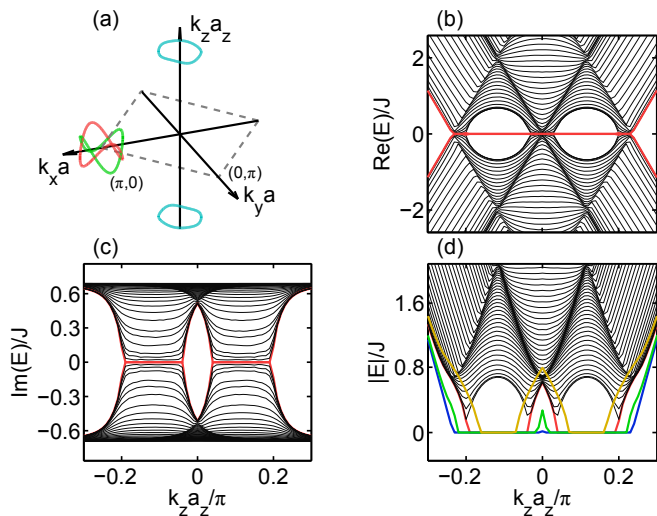


FIG. 3. (Color online) (a) Schematic of Weyl exceptional rings denoted by closed red, green and cyan lines for the system described by the Hamiltonian in Eq. (8). The dashed box depicts the first Brillouin zone. (b) Real (c) imaginary and (d) absolute values of the eigenenergy with respect to $k_z a_z$ for $k_y = 0$ and $\gamma = 0.7J$ when the open boundary condition is imposed along the x direction. The red lines are the surface states. In (d), additional surface states for $\gamma = 0, 0.35J, 0.86J$ are plotted as blue, green and yellow lines respectively. Note that only the parts with zero absolute energy are associated with surface states.

($C_{\theta_{\pm+2\pi}} = -1$) when \mathcal{S} encloses one ring. Around $k_{W\pm}$, the corresponding band contributes $C_{\theta_{\pm}} = -1$ ($C_{\theta_{\pm+2\pi}} = 1$). Furthermore, apart from the Chern number, we can characterize the ring by a quantized Berry phase defined in Eq. (6), i.e., evaluated along a closed trajectory enclosing the Weyl exceptional ring twice for a considered band with a ring.

Another intriguing feature of Weyl semimetals is the existence of a Fermi arc, surface states that connect two Weyl points with opposite Chern numbers in a geometry with edges. When $\gamma > 0$, Weyl points develop into Weyl exceptional rings, and one may wonder on the existence of surface states with open boundaries. Here, we calculate the spectra of the open system under open boundaries along the x direction and plot the real, imaginary and absolute parts of the spectra in Fig. 3(b), (c), and (d), respectively. We neglected the spin-independent energy $\hbar^2 k_z^2/2m$ for clarity. Interestingly, zero energy states emerge for both real and imaginary parts of the spectra. Yet, the surface states (Fermi arc) are only associated with those of zero absolute energy, which connect the Weyl exceptional ring at the center (\mathbf{k}_{W0}) to those on two sides ($\mathbf{k}_{W\pm}$). These states are doubly degenerate eigenvectors (not generalized ones [46, 47]), one (the other) of which is localized on the left (right) surface. Compared to the surface states without γ , their range along k_z decreases with respect to γ because the size of the

rings along the z direction grows with γ . Fig. 3(d) shows the shrinking surface states for $\gamma = 0, 0.35J, 0.7J$ and $0.86J$. As γ becomes sufficiently large, the rings around $(k_x a_x, k_y a_y) = (0, 0)$ overlap with those around $(\pi, 0)$ in the k_z direction and surface states completely disappear.

To measure the Weyl exceptional ring, a possible approach is to probe the dynamics of atom numbers of each spin component after a quench [40]. Initially, if we only keep the spin-independent optical lattices but switch off the spin-dependent ones (contributing to the spin-orbit coupling) and dissipation, we can load spin up atoms into the system and the ground state is $\Psi(\mathbf{k} = 0, t = 0) = (1 \ 0 \ 1 \ 0)/\sqrt{2}$ since the Hamiltonian reduces to $H = -\hbar_t \tau_x$. This state can be driven to a state with $\mathbf{k} \neq 0$ by accelerating the optical lattices or by applying an external gradient force. After that, the spin-orbit coupling and dissipation can be suddenly turned on. So this state is no longer the eigenstate of the system and the atom numbers will change with time. For example, if \mathbf{k} lies in the $b_{z-} = 0$ plane, the normalized atom number for spin down is given by

$$n_{\downarrow} = \frac{b_x^2 + b_y^2}{4|E_{\theta}|^2} \left[\sum_{\lambda=\pm} e^{\lambda 2\text{Im}(E_{\theta})t/\hbar} - 2 \cos\left(\frac{2\text{Re}(E_{\theta})t}{\hbar}\right) \right], \quad (9)$$

where $n_{\downarrow} = N_{\downarrow} e^{\gamma t/\hbar}$ with N_{\downarrow} being the atom number. Outside of the ring, $\text{Im}(E_{\theta}) = 0$ and $n_{\downarrow} = (b_x^2 + b_y^2) \sin^2(E_{\theta}t/\hbar)/E_{\theta}^2$ with an oscillation period of $2\pi\hbar/E_{\theta}$ and inside the ring $\text{Re}(E_{\theta}) = 0$ and $n_{\downarrow} = (b_x^2 + b_y^2) [|\sum_{\lambda=\pm} e^{\lambda 2\text{Im}(E_{\theta})t/\hbar} - 2| / (4|E_{\theta}|^2)]$ with no oscillation. The existence of the Weyl exceptional ring will be manifested through the change in oscillation periods. In experiments, one may choose ^{87}Rb (bosons) atoms and apply blue-detuned laser beams at wavelength $\lambda = 767 \text{ nm}$ [48] to generate the optical lattices with Weyl points. With specific experimental settings, our model parameters are given by $J_{SO} = 0.5J$ and $J = 0.058E_R$, where the recoil energy is $E_R/\hbar = \hbar k_R^2/2m = 2\pi \times 3.9 \text{ kHz}$ with $k_R = 2\pi/\lambda$ and λ being the wavelength of laser beams. The decay strength γ can be experimentally tuned by controlling the intensity of the resonant optical beam.

In summary, we have discovered a Weyl exceptional ring in a dissipative system of Weyl points with particle gain and loss. Such a ring is characterized by both a quantized Chern number and a quantized Berry phase, which are defined via the Riemann surface. We further propose an experimental scheme in cold atoms to realize the Weyl exceptional ring, which paves the way for future experimental investigation of such a ring and its unusual topological properties.

We thank S. A. Yang for helpful discussions. This work was supported by the ARL, the IARPA LogiQ program, and the AFOSR MURI program.

* yongxuph@umich.edu

- [1] A. A. Burkov, Nat. Mater. **15**, 1145 (2016).
 [2] S. Jia, S.-Y. Xu, and M. Z. Hasan, Nat. Mater. **15**, 1140 (2016).
 [3] A. A. Burkov, M. D. Hook, and L. Balents, Phys. Rev. B **84**, 235126 (2011).
 [4] Y. Xu, F. Zhang, and C. Zhang, Phys. Rev. Lett. **115**, 265304 (2015).
 [5] A. A. Soluyanov, D. Gresch, Z. Wang, Q. Wu, M. Troyer, X. Dai, and B. A. Bernevig, Nature **527**, 495 (2015).
 [6] B. Bradlyn, *et al.*, Science, **353**, 6299 (2016).
 [7] X. Wan, A. M. Turner, A. Vishwanath, and S. Y. Savrasov, Phys. Rev. B **83**, 205101 (2011).
 [8] K.-Y. Yang, Y.-M. Lu, and Y. Ran, Phys. Rev. B **84**, 075129 (2011).
 [9] A. A. Burkov and L. Balents, Phys. Rev. Lett. **107**, 127205 (2011).
 [10] G. Xu, H. Weng, Z. Wang, X. Dai, and Z. Fang, Phys. Rev. Lett. **107**, 186806 (2011).
 [11] M. Gong, S. Tewari, and C. Zhang, Phys. Rev. Lett. **107**, 195303 (2011).
 [12] B. M. Anderson, G. Juzeliunas, V. M. Galitski, and I. B. Spielman, Phys. Rev. Lett. **108**, 235301 (2012).
 [13] L. Lu, L. Fu, J. D. Joannopoulos, and M. Soljačić, Nat. photon. **7**, 294 (2013).
 [14] S. A. Yang, H. Pan, and F. Zhang, Phys. Rev. Lett. **113**, 046401 (2014).
 [15] Y. Xu, R.-L. Chu, and C. Zhang, Phys. Rev. Lett. **112**, 136402, (2014).
 [16] T. Dubček, C. J. Kennedy, L. Lu, W. Ketterle, M. Soljačić, and H. Buljan, Phys. Rev. Lett. **114**, 225301 (2015).
 [17] B. Liu, X. Li, L. Yin, and W. V. Liu, Phys. Rev. Lett. **114**, 045302 (2015).
 [18] H. Ishizuka, T. Hayata, M. Ueda, and N. Nagaosa, arXiv:1607.06537 (2016).
 [19] S.-Y. Xu, *et al.*, Science **349**, 613 (2015).
 [20] B. Q. Lv, *et al.*, Phys. Rev. X **5**, 031013 (2015).
 [21] L. Lu, Z. Wang, D. Ye, L. Ran, L. Fu, J. D. Joannopoulos, and M. Soljačić, Science **349**, 622 (2015).
 [22] G. E. Volovik, The Universe in a Helium Droplet (Clarendon Press, Oxford, 2003).
 [23] G. Bian, *et al.*, Nat. Commun. **7**, 10556 (2016).
 [24] Y. Xu and C. Zhang, Phys. Rev. A **93**, 063606 (2016).
 [25] D.-W. Zhang, Y. X. Zhao, R.-B. Liu, Z.-Y. Xue, S.-L. Zhu, and Z. D. Wang, Phys. Rev. A **93**, 043617 (2016).
 [26] N. Moiseyev, Non-Hermitian Quantum Mechanics (Cambridge Univ. Press, 2011).
 [27] I. Rotter, J. Phys. A **42**, 153001 (2009).
 [28] M. Berry, Czech. J. Phys. **54**, 1039 (2004).
 [29] W. D. Heiss, J. Phys. A **45**, 44 (2012).
 [30] A. Guo, *et al.*, Phys. Rev. Lett. **103**, 093902 (2009).
 [31] C. E. Rüter, K. G. Makris, R. El-Ganainy, D. N. Christodoulides, M. Segev, and D. Kip, Nat. Phys. **6**, 192 (2010).
 [32] Y. Chong, L. Ge, and A. D. Stone, Phys. Rev. Lett. **106**, 093902 (2011).
 [33] M. Liertzer, Li Ge, A. Cerjan, A. D. Stone, H. E. Türeci, and S. Rotter, Phys. Rev. Lett. **108**, 173901 (2012).
 [34] M. Müller, S. Diehl, G. Pupillo, and P. Zoller, Adv. At. Mol. Opt. Phys. **61**, 1 (2012).
 [35] B. Peng, *et al.*, Nat. Phys. **10**, 394 (2014).
 [36] L. Feng, Z. J. Wong, R.-M. Ma, Y. Wang, and X. Zhang, Science **346**, 972 (2014).
 [37] H. Hodaei, M.-A. Miri, M. Heinrich, D. N. Christodoulides, and M. Khajavikhan, Science **346**, 975 (2014).
 [38] B. Zhen, *et al.*, Nature **525**, 354 (2015).
 [39] T. Gao, *et al.*, Nature **526**, 554 (2015).
 [40] J. Li, A. K. Harter, J. Liu, L. de Melo, Y. N. Joglekar, and L. Luo, arXiv:1608.05061 (2016).
 [41] C. M. Bender and S. Boettcher, Phys. Rev. Lett. **80**, 5243(1998).
 [42] M. Klemm and O. D. Lavrentovich, Soft Matter Physics: An Introduction
 [43] D. Xiao, M.-C. Chang, and Q. Niu, Rev. Mod. Phys. **82**, 1959 (2010).
 [44] G. Sundaram and Q. Niu, Phys. Rev. B **59**, 14915 (1999).
 [45] Y. Xu and L.-M. Duan, arXiv:1607.04924 (2016).
 [46] T. E. Lee, Phys. Rev. Lett. **116**, 133903 (2016).
 [47] D. Leykam, K. Y. Bliokh, C. Huang, Y. D. Chong, and F. Nori, arXiv:1610.04029 (2016).
 [48] Z. Wu, *et al.*, Science **354**, 83 (2016).

SUPPLEMENTAL MATERIAL

In the supplemental material, we will derive the semiclassical equation for a wave packet in an optical lattice with a non-Hermitian term. The wave packet can be constructed from Bloch wave functions:

$$|\Phi\rangle = \int d\mathbf{k} a(\mathbf{k}, t) |\phi_n(\mathbf{k})\rangle, \quad (\text{S1})$$

where $|\phi_n(\mathbf{k})\rangle$ is a right Bloch wave function of H_C , the Hamiltonian describing the system, i.e., $H_C|\phi_n(\mathbf{k})\rangle = E_n(\mathbf{k})|\phi_n(\mathbf{k})\rangle$ with $|\phi_n(\mathbf{k})\rangle = e^{i\mathbf{k}\cdot\mathbf{r}}|u_n(\mathbf{k})\rangle$, $\langle u_n(\mathbf{k})|u_n(\mathbf{k})\rangle = 1$ and n being the band index; $a(\mathbf{k}, t) = |a(\mathbf{k}, t)|e^{i\gamma(\mathbf{k}, t)}$ with the amplitude $|a(\mathbf{k}, t)|$ taking the Gaussian form centered at $\mathbf{k}_c = \int d\mathbf{k} |a'(\mathbf{k}, t)|^2 \mathbf{k} / \int d\mathbf{k} |a'(\mathbf{k}, t)|^2$ with $|a'(\mathbf{k}, t)|^2 \equiv |a(\mathbf{k}, t)|^2 / \int d\mathbf{k}' |a(\mathbf{k}', t)|^2$ and the phase $\gamma(\mathbf{k}, t)$ incorporating a dynamical and Berry phase. Since we only consider the case that a single band is occupied by the wave packet, we will neglect the subscript n hereafter.

Using Eq. (S1), the location of the wave packet is given by

$$\begin{aligned} \mathbf{r}_c &= \langle \Phi | \hat{\mathbf{r}} | \Phi \rangle / \langle \Phi | \Phi \rangle \\ &= - \int d\mathbf{k} |a'(\mathbf{k}, t)|^2 \partial_{\mathbf{k}} \gamma(\mathbf{k}, t) + \int d\mathbf{k} |a'(\mathbf{k}, t)|^2 \langle u(\mathbf{k}) | i \partial_{\mathbf{k}} | u(\mathbf{k}) \rangle \end{aligned} \quad (\text{S2})$$

$$\approx -\partial_{\mathbf{k}_c} \gamma(\mathbf{k}_c, t) + \mathbf{A}(\mathbf{k}_c), \quad (\text{S3})$$

where $\mathbf{A}(\mathbf{k}_c) = i \langle u(\mathbf{k}_c) | \partial_{\mathbf{k}_c} | u(\mathbf{k}_c) \rangle$ and $\gamma(\mathbf{k}_c, t) = - \int_{t_0}^t dt' \text{Re} \left[E_{\mathbf{k}_c(t')} - \tilde{\mathbf{A}}(\mathbf{k}_c(t')) \cdot \frac{d\mathbf{k}_c}{dt'} \right]$ with $\tilde{\mathbf{A}}(\mathbf{k}_c) = i \langle \tilde{u}(\mathbf{k}_c) | \partial_{\mathbf{k}_c} | u(\mathbf{k}_c) \rangle$, where the first and second terms correspond to the dynamical and Berry phases, respectively. Using Eq. (S3), we can obtain the semiclassical equation in terms of a velocity

$$\mathbf{v}_c(t_0) = \lim_{\delta t \rightarrow 0} \frac{\mathbf{r}_c(t_0 + \delta t) - \mathbf{r}_c(t_0)}{\delta t} = \partial_{\mathbf{k}_c} \bar{E}(\mathbf{k}_c) - \dot{\mathbf{k}}_c \times \boldsymbol{\Omega}(\mathbf{k}_c) \quad (\text{S4})$$

with $\bar{E}(\mathbf{k}_c) = \text{Re}[E(\mathbf{k}_c)] + \tilde{\mathbf{A}}(\mathbf{k}_c) \cdot \dot{\mathbf{k}}_c$.
